

Convex X-ray Spectra of PKS 2155-304 and Constraints on the Minimum Electron Energy

Sitha K. Jagan^{1*}, S. Sahayanathan^{2†}, Frank M. Rieger^{3,4‡} and C. D. Ravikumar¹

¹*Department of Physics, University of Calicut, Malappuram-673635, India*

²*Astrophysical Sciences Division, Bhabha Atomic Research Centre, Mumbai - 400085, India*

³*ZAH, Institute of Theoretical Astrophysics, University of Heidelberg, Philosophenweg 12, 69120 Heidelberg, Germany*

⁴*Max-Planck-Institut für Kernphysik, P.O. Box 103980, 69029 Heidelberg, Germany*

Accepted XXX. Received YYY; in original form ZZZ

ABSTRACT

The convex (concave upward) high-energy X-ray spectra of the blazar PKS 2155-304, observed by *XMM-Newton*, is interpreted as the signature of sub-dominant inverse Compton emission. The spectra can be well fitted by a superposition of two power-law contributions which imitate the emission due to synchrotron and inverse Compton processes. The methodology adopted enables us to constrain the photon energy down to a level where inverse Compton emission begins to contribute. We show that this information supplemented with knowledge of the jet Doppler factor and magnetic field strength can be used to constrain the low-energy cutoff $\gamma_{\min} m_e c^2$ of the radiating electron distribution and the kinetic power P_j of the jet. We deduce these quantities through a statistical fitting of the broadband spectral energy distribution of PKS 2155-304 assuming synchrotron and synchrotron self Compton emission mechanisms. Our results favour a minimum Lorentz factor for the non-thermal electron distribution of $\gamma_{\min} \gtrsim 60$, with a preference for a value around $\gamma_{\min} \approx 330$. The required kinetic jet power is of the order of $P_j \sim 3 \times 10^{45}$ erg s⁻¹ in case of a heavy, electron-proton dominated jet, and could be up to an order of magnitude less in case of a light, electron-positron dominated jet. When put in context, our best fit parameters support the X-ray emitting part of blazar jets to be dominated by an electron-proton rather than an electron-positron composition.

Key words: acceleration of particles – radiation mechanisms: non-thermal – galaxies: BL Lacertae objects: individual: PKS 2155-304 – X-rays: galaxies – X-rays: individual: PKS 2155-304

1 INTRODUCTION

A prominent morphological feature of the radio-loud type AGN is the presence of relativistic jets extending up to megaparsec scales. Blazars are the class of radio-loud AGN in which the jet is aligned close to the line of sight of the observer. Hence the emission from blazars is significantly Doppler-boosted. Their spectrum is predominantly non-thermal in nature, extending from radio to GeV and TeV energies (e.g., [Abdo et al. 2010](#); [Reimer & Böttcher 2013](#)). Blazars are further classified into flat spectrum radio quasars (FSRQs) or BL Lac type objects (BL Lacs) depending upon the presence or absence of emission line features. The spectral energy distribution (SED) of blazars is typically characterized by a double-hump structure with the low-energy component peaking around IR/optical/UV energies and the high-energy component peaking around gamma-ray energies (e.g., [Fossati et al. 1998](#); [Ghisellini et al. 2017](#)). The low-energy emission is well understood to be synchrotron emission from

a relativistic non-thermal electron distribution; whereas, the high-energy emission is often interpreted as due to inverse Compton (IC) scattering of low-energy photons by the same electron distribution (e.g., [Maraschi et al. 1992](#); [Marscher & Gear 1985](#); [Begelman et al. 1987](#); [Dermer & Schlickeiser 1993](#)). The peak energy of the synchrotron spectral component is used to sub-divide BL Lacs into low energy peaked BL Lacs (LBLs: peaking at IR/optical), intermediate energy peaked BL Lacs (IBLs: peaking at optical/UV) and high energy peaked BL Lacs (HBLs: peaking at UV/soft X-ray) ([Padovani & Giommi 1995](#); [Fossati et al. 1998](#)). Within the leptonic framework, the gamma-ray spectra of HBLs are well reproduced by synchrotron self-Compton (SSC) emission. The target photons for the IC scattering in this case are the synchrotron photons themselves.

Spectral modelling of HBLs by synchrotron and SSC processes suggests that the underlying electron distribution may be closely related to a power-law/broken power-law type function resulting from Fermi acceleration and radiative cooling processes (e.g., [Kirk et al. 1998](#); [Kirk & Mastichiadis 1999](#)). However, high resolution X-ray spectra can exhibit significant deviations from a power-law and are often better reproduced by a log-parabola function ([Massaro et al.](#)

* E-mail: sithajagan@gmail.com

† E-mail: sunder@barc.gov.in

‡ E-mail: frank.rieger@mpi-hd.mpg.de

2008). Such curved spectra demand a modified electron distribution which can be achieved by assuming energy-dependent acceleration or particle diffusion time scales (Tramacere et al. 2011, 2007; Jagan et al. 2018; Goswami et al. 2020).

Even after substantial progress in understanding the emission processes in blazars, the matter content and kinetic power of blazar jets are still open questions (e.g., Celotti & Ghisellini 2008; Madejski et al. 2016; Ghisellini et al. 2014; Zdziarski & Bottcher 2015). Though the detection of neutrinos provides indications for the presence of hadrons in blazar jets (IceCube Collaboration et al. 2018; Tavecchio et al. 2014), their signature in the emission spectra is largely unknown since models advocating a hadronic origin of high-energy spectra pose serious energy constraints (Zdziarski & Bottcher 2015). Leptonic models are largely successful in explaining the broadband SED of blazars especially during the flare. These models generally assume the protons to be cold and contribute only to the jet kinetic power (Celotti & Ghisellini 2008). However, if their number is equal to that of the non-thermal electrons (heavy jet), the predicted jet power could exceed the accretion disk luminosity (Ghisellini et al. 2014).

For a power-law or power-law type electron distribution $N(\gamma)$ of index $p > 1$, the total electron number density N_{tot} is determined by the differential number density at the minimum cut-off energy γ_{min} , i.e., $N_{\text{tot}} \approx N(\gamma_{\text{min}}) \gamma_{\text{min}} / (p-1)$, γ being the electron Lorentz factor. Under a Fermi-type acceleration process, this energy can be related to the energy of the electron population injected into the acceleration region (Kirk et al. 1998; Kusunose & Takahara 2018). As mentioned earlier, the knowledge of the total electron number density can also provide an estimate of the blazar jet mass density by assuming an appropriate fraction of hadrons. This, along with broadband spectral modelling, can provide clues on the kinetic power of blazar jets. However, the estimation of γ_{min} based on spectral information is complicated by the fact that the related synchrotron emission usually falls into the radio regime which is significantly self-absorbed or contaminated by extended jet emission. On the other hand, the low-energy IC contribution may be overwhelmed by the dominant synchrotron emission. Still, an upper limit on the related minimum IC photon energy might be estimated from the transition energy in the broadband spectra, where the dominant contribution shifts from synchrotron to IC emission (Kataoka & Stawarz 2016).

PKS 2155-304 is a HBL located at a redshift of $z = 0.116$ and well observed from radio to very high energy (VHE) gamma rays. Its synchrotron spectrum peaks at UV and the IC spectral component peaks at GeV energies (Zhang 2008; Madejski et al. 2016). Its broadband spectra can be reproduced reasonably well by synchrotron and SSC emission of a broken power-law type electron distribution (Madejski et al. 2016; Abdalla et al. 2020). The source is known to exhibit rapid variability with doubling time as short as a few minutes, suggesting that the emission region is located very close to the supermassive black hole powering the AGN (Aharonian et al. 2007; Rieger & Volpe 2010).

The mild curvature observed in the high resolution X-ray spectra can be interpreted as an outcome of the energy-dependence of the particle escape time-scale. However, during certain epochs, the X-ray spectral curvature reverses the sign indicating a convex (concave upward) spectrum suggesting the spectral contribution of a sub-dominant IC component in addition to the synchrotron component (Jagan et al. 2018).

The contribution of IC emission to the X-ray spectra of PKS 2155-304 can be inferred from *XMM-Newton* observation, where the spectrum has been found to harden beyond 4 keV. This

was first shown by Zhang (2008), who used a broken power-law spectral fit to highlight the presence of an IC component. *NuSTAR* observations of PKS 2155-304 at 0.5-60 keV also reveal that the IC spectral component dominates over the synchrotron spectrum beyond ≈ 6 keV (Madejski et al. 2016). This has been demonstrated by fitting the spectrum with a broken power-law, a combination of two power-law functions (double power-law) and log parabola-power-law combination, respectively. *NuSTAR* observation of yet another HBL, MKN 421 also showed a convex X-ray spectrum during a low-flux state that can be well reproduced by a double power-law function (Kataoka & Stawarz 2016). In general, the presence of convex X-ray spectra has also been witnessed for many IBLs and LBLs and are interpreted as the signature of the IC spectral component (e.g., Tagliaferri et al. 2000; Tanihata et al. 2003; Wiercholska & Wagner 2016; Gaur et al. 2018).

Alternatively, a convex X-ray spectrum may also be an outcome of a high energy pile-up of the emitting electron distribution. Such a high energy excess in the electron distribution can occur in at least two scenarios. When the confinement time of the electrons in the region of particle acceleration is much longer than the radiative loss timescales, the electrons will eventually get accumulated at the maximum energy giving rise to a relativistic Maxwellian tail at high energies (e.g., Schlickeiser 1985; Ostrowski 2000; Stawarz & Petrosian 2008; Lefa et al. 2011). Another scenario could be, when the electron energy loss rate at high energy is dominated by IC scattering of the external photon field happening in the Klein-Nishina regime (Dermer & Atoyan 2002; Moderski et al. 2005).

While in the case of PKS 2155-304 the high energy emission is thought to be dominated by SSC processes rather than external Compton, it is often not straightforward to differentiate the process responsible for the convex X-ray spectra. Nevertheless, the contribution of a sub-dominant Compton spectral component can be identified through a statistical study between the X-ray spectral curvature and the simultaneous low energy gamma-ray spectral index of the Compton spectrum.

In the present work, we perform a detailed study of the convex X-ray spectra of PKS 2155-304 observed by *XMM-Newton*. The convexness observed in the 0.6-10 keV X-ray spectrum is interpreted as the signature of a sub-dominant SSC contribution. We extend this along with broadband spectral modelling to constrain the low-energy cut-off of the emitting electron distribution and the source energetics.

The paper is organised as follows: In § 2, we explain the observations and data reduction procedure. Epochs during which the X-ray spectrum is convex are identified in § 3. In § 4 and 5, we show that this can be interpreted as the result of a combination of synchrotron and SSC spectral components using a double power-law function. In § 6 we describe the broadband spectral fitting of the source and the estimation of jet power. The outcome is discussed in § 7. Throughout this work, we adopt a cosmology with $\Omega_m = 0.3$, $\Omega_\Lambda = 0.7$ and $H_0 = 70 \text{ km s}^{-1} \text{ Mpc}^{-1}$.

2 OBSERVATIONS AND DATA REDUCTION

PKS 2155-304 has been observed extensively by *XMM-Newton*, with 37 *XMM-Newton* master observations available in the *HEASARC* archive from 2000-2014. For our X-ray study, we have taken the *XMM-Newton*'s European Photon Imaging Camera (EPIC)-PN data only and avoided EPIC-MOS data. The reason for this being less sensitivity and quantum efficiency, and the chance of

pile up in EPIC-MOS data during the observation of bright sources. Among 37 *XMM-Newton* observations, only 22 PN observations were available during which the camera was operated in the small window imaging mode. The *XMM-Newton* Science Analysis System (SAS version 14.0) with the latest calibration files was used for the data reduction.

The standard procedures were followed to reprocess the Observation Data File (ODF). The *XMM-Newton* SAS pipeline command *epchain* is used to produce the calibrated photon event files for the PN camera. In the selected 0.2-10.0 keV energy range, we considered both single and double events ($\text{PATTERN} \leq 4$) of PN data which were flagged good quality ($\text{FLAG}=0$) for processing. We extracted the light curves in the high energy range 10-12 keV in order to check the background particle flaring. An appropriate threshold rate was chosen from the light curve to omit the background flaring period and a ‘‘good time interval (GTI)’’ event list was created. A circular region of size $40''$ around the source was selected for extracting the source spectrum and two circular regions of the same size were chosen as the background. These background regions were selected from the same CCD chip of source region such that the source photon contribution was negligible within these regions.

The chance of pile up is more probable for bright sources like PKS 2155-304 and hence, we used the SAS task *epatplot* to examine the pile up effect in all observations. We found that certain observations are affected by the pile up. In order to avoid these pile up effects, we considered an annulus region around the bright source with an inner radius of $10''$ and outer radius varying from $38''$ to $40''$. The range of the outer radius was chosen such that the source selection region remained within the frame of the CCD chip. Only the annulus region was taken into account for source count extraction and the inner region was excluded.

The SAS tool *specgroup* was used for grouping the spectral channels. We imposed a condition of having minimum 100 counts in each group. PKS 2155-304 being a bright source, there can be large number of counts in the spectrum which in turn results in large number of bins. To avoid the chance of oversampling, we fixed the oversampling value to 5 so that the energy resolution cannot be covered by more than 5 grouped bins. The Galactic hydrogen column density ($N_{\text{H}} = 1.71 \times 10^{20} \text{ cm}^{-2}$) toward PKS 2155-304 was kept constant for all spectral fits (Bhagwan et al. 2014).

We also used the simultaneous optical observation of the source by Optical Monitor (OM) onboard *XMM-Newton*. Reprocessing of the OM data was carried out by the SAS metatask *omichain*. From the combined source list, our source of interest was obtained by cross matching its RA and Dec with the coordinates of all sources in the list. Unlike X-rays, optical/UV photons from the jet can be contaminated by the galactic photons at the same wavelength. This was treated as systematic error, and similar to Jagan et al. (2018), it was estimated by fitting the optical/UV data by a power-law function. We found that adding 3 per cent systematic error in most of the data sets led to a better fit statistics. However, we had to reject 6 observations which either demanded higher systematic errors or lacked a minimum of 3 optical/UV flux points to perform the statistical fit. Finally, we got 16 observations which are used for the present study. Among these observations we selected only those observations which showed convex X-ray spectra (see § 3). The details of these observations are given in Table 3. The galactic reddening correction was done for all the optical/UV data using the model *UVRED* and fixing the parameter $E_{\text{B}-\text{V}} = 0.019$ (Seaton 1979; Schlafly & Finkbeiner 2011).

3 X-RAY SPECTRAL CURVATURE

To identify the X-ray spectral curvature of PKS 2155-304, the 22 epochs of *XMM-Newton* PN observations over the energy range 0.6-10.0 keV were fitted with the X-ray Spectral Fitting Package (XSPEC) (Arnaud 1996) using a log-parabola function (Massaro et al. 2004). This function is defined as

$$F_{\text{lp}}(\epsilon) = F_{\text{p}} \left(\frac{\epsilon}{\epsilon_{\text{p}}} \right)^{-\alpha - \beta \log(\epsilon/\epsilon_{\text{p}})}, \quad (1)$$

where ϵ is the photon energy (keV), F_{p} is the flux ($\text{photons cm}^{-2} \text{ s}^{-1} \text{ keV}^{-1}$) at photon energy ϵ_{p} and the spectral shape is determined by the two parameters α and β . The parameter α governs the spectral slope at ϵ_{p} and β is the parameter defining the spectral curvature. A negative value of β indicates a convex spectrum that could hint at the presence of Compton spectral component or a high energy excess in the underlying electron distribution. In the 0.6-10.0 keV regime the spectrum of PKS 2155-304 is dominated by the high energy end of the synchrotron emission, so that any IC contribution can result in mild negative value of β .

The log-parabola spectral fit to most of the observations resulted in positive β suggesting a convex spectrum (Jagan et al. 2018). Among the 22 observations, four (IDs 0158961401, 0411780101, 0411780201 and 0411780701) have negative β values indicative of a convex nature. The best fit parameters during these epochs are given in Table 1. For three observations (0158961401, 0411780101 and 0411780201) the negative values of β are statistically significant.

4 COMPTON SPECTRAL SIGNATURE IN X-RAY SPECTRA

To explore the contribution of a Compton component in the X-ray spectra of PKS 2155-304, we assume that the synchrotron and SSC spectra at 0.6-10.0 keV can each be represented by a power-law. Accordingly, the cumulative spectrum (νF_{ν}) will be a double power-law defined by

$$F_{\text{dp}}(\epsilon) = F_0 \left[\left(\frac{\epsilon}{\epsilon_{\text{m}}} \right)^{-\Gamma_{\text{syn}}} + \left(\frac{\epsilon}{\epsilon_{\text{m}}} \right)^{\Gamma_{\text{com}}} \right], \quad (2)$$

where ϵ_{m} is the photon energy at which the fluxes due to synchrotron and SSC processes are equal to F_0 , and $-\Gamma_{\text{syn}}$ and Γ_{com} are the synchrotron and SSC spectral indices, respectively.

Applying this, we find that the convex X-ray spectra of PKS 2155-304, corresponding to the observation IDs 0158961401, 0411780101 and 0411780201 can be well-fitted with a double power-law function. However, a direct comparison between the fit statistics of the double power-law and the log-parabola functions cannot be done due to the difference in the number of free parameters. The log-parabolic spectrum (eq. 1) is governed by three parameters (F_{p} , α and β), while the double power-law spectrum is governed by four parameters (F_0 , ϵ_{m} , Γ_{syn} and Γ_{com}). To progress, we reduce the number of free parameters of the double power-law function to three by fixing Γ_{com} at a value equal to the best fit spectral index of the simultaneous optical/UV spectrum. The rationale behind this being, if the 0.6-10.0 keV SSC spectrum is produced by the same power-law electron distribution responsible for the optical/UV emission also, then in the Thomson scattering regime both spectral indices will be equal. By this approach, the number of free parameters of the double power-law model is made equal to that of

Obs. ID	Date of Observation (yyyy.mm.dd)	logpar			
		α	β	norm(10^{-5})	χ^2_{red} (dof)
0158961401	2006-05-01	2.63 ± 0.01	-0.10 ± 0.02	14.97 ± 0.06	1.06(173)
0411780101	2006-11-07	2.58 ± 0.01	-0.10 ± 0.02	19.41 ± 0.06	1.01(184)
0411780201	2007-04-22	2.70 ± 0.01	-0.04 ± 0.01	46.32 ± 0.10	1.11(248)
0411780701	2012-04-28	2.90 ± 0.01	-0.02 ± 0.03	5.63 ± 0.02	1.11(149)

Table 1. Log-parabola spectral fit results (photons $\text{cm}^{-2} \text{s}^{-1} \text{keV}^{-1}$) for the epochs with convex X-ray spectra (pivot energy fixed at 1 keV).

the log-parabola so that, a direct comparison of fit statistics is possible. The results of fit are given in Table 3 and show that a double power-law model can also explain the convex X-ray spectrum as compared to a log-parabola model. The X-ray spectral curvature of PKS 2155-304 has also been studied by Gaur et al. (2017). Their study also indicated the convex nature of the X-ray spectrum corresponding to the observation ID 0411780701. However, the F-test result suggests this curvature to be minimal. In addition to the χ^2 test, we have performed F-test to obtain the statistical significance of log-parabola or double power-law. This analysis is performed for all the observations and the test results are given in Table 2. We also find that the log-parabola spectral fit to the observation ID 0411780701 do not show any significant improvement over the simple power-law. Hence, we have excluded this observation from the rest of the study.

In principle, the spectral slope and the concavity of the double power-law function can be obtained from the first and second derivatives of $\log F_{\text{dp}}$ with respect to $\log \epsilon$, i.e.,

$$\log F'_{\text{dp}} \equiv \frac{d(\log F_{\text{dp}})}{d(\log \epsilon)} = \left(\frac{-\Gamma_{\text{syn}} x_m^{-\Gamma_{\text{syn}}} + \Gamma_{\text{com}} x_m^{\Gamma_{\text{com}}}}{x_m^{-\Gamma_{\text{syn}}} + x_m^{\Gamma_{\text{com}}}} \right) \quad (3)$$

$$\log F''_{\text{dp}} \equiv \frac{d^2(\log F_{\text{dp}})}{d(\log \epsilon)^2} = \frac{(\Gamma_{\text{com}} + \Gamma_{\text{syn}})^2 x_m^{-\Gamma_{\text{syn}} + \Gamma_{\text{com}}}}{[x_m^{-\Gamma_{\text{syn}}} + x_m^{\Gamma_{\text{com}}}]^2} > 0, \quad (4)$$

where $x_m = \epsilon/\epsilon_m$. The positive value of the second derivative reaffirms the convex nature of the chosen double power-law function. The curvature κ_{dp} of the double power-law function is given by

$$\kappa_{\text{dp}} = \frac{\log F''_{\text{dp}}}{(1 + \log F'_{\text{dp}})^2} = \frac{(\Gamma_{\text{com}} + \Gamma_{\text{syn}})^2 (x_m^{-\Gamma_{\text{syn}}} + x_m^{\Gamma_{\text{com}}}) x_m^{-\Gamma_{\text{syn}} + \Gamma_{\text{com}}}}{\left[(x_m^{-\Gamma_{\text{syn}}} + x_m^{\Gamma_{\text{com}}})^2 + (\Gamma_{\text{syn}} x_m^{-\Gamma_{\text{syn}}} - \Gamma_{\text{com}} x_m^{\Gamma_{\text{com}}})^2 \right]^{3/2}}. \quad (5)$$

The valley energy ϵ_v , corresponding to the minimum flux in the νF_ν representation can be obtained by setting equation (3) to zero, yielding

$$\epsilon_v = \epsilon_m \left(\frac{\Gamma_{\text{syn}}}{\Gamma_{\text{com}}} \right)^{\frac{1}{\Gamma_{\text{syn}} + \Gamma_{\text{com}}}}. \quad (6)$$

From equation (5), κ_{dp} for the case $x_m \ll 1$ will be

$$\kappa_{\text{dp}}(x_m \ll 1) \approx \frac{(\Gamma_{\text{syn}} + \Gamma_{\text{com}})^2}{(1 + \Gamma_{\text{syn}}^2)^{3/2}} x_m^{\Gamma_{\text{syn}} + \Gamma_{\text{com}}}. \quad (7)$$

Hence in this case, $\kappa_{\text{dp}}(x_m \ll 1)$ will decrease with increasing $\Gamma_{\text{syn}} + \Gamma_{\text{com}}$. As mentioned before, the optical/UV spectral index could be used as an approximation for Γ_{com} while for Γ_{syn} we used the results from the double power-law fitting. For the observation

0411780701, Γ_{syn} was obtained through a simple power-law fit (Table 3). We calculated the X-ray spectral curvature at 1 keV using the log-parabola model instead of double power-law. This is to avoid any possible bias as Γ_{syn} was also estimated assuming a double power-law. In case of a log-parabolic function, the curvature in νF_ν representation can be obtained as

$$\kappa_{\text{lp}} = - \frac{2\beta}{\left\{ 1 + \left[2 - \alpha - 2\beta \log \left(\frac{\epsilon}{\epsilon_p} \right) \right]^2 \right\}^{3/2}}. \quad (8)$$

We then study the dependence of κ_{lp} on the sum of optical/UV and X-ray spectral indices. This is done by redefining the log-parabola function in terms of κ_{lp} using equation (8) and adding it as a local model in XSPEC. The best fit κ_{lp} values are given in column 7 of Table 3. As can be seen, the spectral curvature can be as high as 0.15. Equation (7) suggests that $\log(\kappa_{\text{lp}})$ varies linearly with $\Gamma_{\text{syn}} + \Gamma_{\text{com}}$. In Figure 1, we plot these quantities and the least square fit, considering both the uncertainties (Press et al. 1992), yielding $a = 0.64 \pm 0.14$ and $b = -0.28 \pm 0.12$ with a goodness-of-fit (Q-value) of 0.89¹. Hence, this result supports our inference that the convex X-ray spectra of PKS 2155-304 is an outcome of the superposition of a synchrotron and a SSC emission component.

In order to explore the minimum photon energy (ϵ_{min}) that could observationally be associated with SSC emission, we modify equation (2) as

$$F_{\text{dp}}(\epsilon) = F_0 \left[\left(\frac{\epsilon}{\epsilon_m} \right)^{-\Gamma_{\text{syn}}} + \left(\frac{\epsilon}{\epsilon_m} \right)^{\Gamma_{\text{com}}} \Theta(\epsilon - \epsilon_{\text{min}}) \right] \quad (9)$$

where Θ is a Heaviside function. Using equation (9) as a local model in XSPEC, and fixing F_0 , Γ_{syn} and Γ_{com} to their best fit values, we then determined an upper limit $\epsilon_{\text{min},c}$ such that $\epsilon_{\text{min}} < \epsilon_{\text{min},c}$ did not modify the fit statistics. In Table 4, we provide the 1- σ upper limit on the $\epsilon_{\text{min},c}$ and in Figure 2 we show the variation of χ^2_{red} with ϵ_{min} . These findings suggest that the IC power-law can be extended down to at least ≈ 0.6 keV. It is tempting to extend this further down as the *XMM-Newton* EPIC instrument is sensitive from 0.15 keV. However, we focused only on 0.6-10 keV range, since there can be contamination due to low pulse height events at the low energy end of the PN camera.

5 MINIMUM ELECTRON ENERGY AND JET ENERGETICS

Constraints on $\epsilon_{\text{min},c}$ can be used to gain insights into the minimum electron energy γ_{min} of the non-thermal electron distribution responsible for the broadband emission. However, for blazars this de-

¹ We fit a straight line of the form $y = a + bx$ to the set of points $(x_i \pm \Delta x_i, y_i \pm \Delta y_i)$. If Q-value > 0.1 the fit is trustable.

Obs. ID	PL			logpar		double PL	
	P	norm(10^{-3})	χ^2_{red} (dof)	F-test	P-value	F-test	P-value
0158961401	2.59 ± 0.01	15.07 ± 0.05	1.35(174)	49.22	4.95×10^{-11}	50.79	2.67×10^{-11}
0411780101	2.55 ± 0.01	19.58 ± 0.06	1.39(185)	71.01	1.00×10^{-14}	67.29	3.95×10^{-14}
0411780201	2.69 ± 0.00	46.43 ± 0.09	1.19(249)	19.04	1.88×10^{-5}	17.05	4.98×10^{-5}
0411780701	2.89 ± 0.01	5.63 ± 0.02	1.11(150)	0.91	0.34	1.39	0.24

Table 2. Power-law (PL) spectral fit and F-test results for the epochs with convex X-ray spectra. Columns 2 - 4 are the index, normalization and reduced chi square (degrees of freedom) for PL fit. Columns 5 and 6 are the F statistic value and null-hypothesis probability for logparabola against PL model. Columns 7 and 8, are the F statistic value and null-hypothesis probability for double power-law against PL model.

Obs. ID	Γ_{syn}	$\log \epsilon_{\nu}$ (keV)	$F_{0.6-10 \text{ keV}}$	χ^2_{red} (dof)	$\Gamma_{\text{com}}(\chi^2_{\text{red}})$	κ_{lp}
0158961401	0.70 ± 0.03	$1.93^{+0.16}_{-0.14}$	3.88 ± 0.02	1.05(173)	$0.17 \pm 0.06(1.77)$	0.12 ± 0.03
0411780101	0.64 ± 0.02	$1.67^{+0.10}_{-0.08}$	5.28 ± 0.02	1.03(184)	$0.26 \pm 0.06(1.81)$	0.13 ± 0.02
0411780201	0.72 ± 0.01	$2.08^{+0.25}_{-0.12}$	12.78 ± 0.03	1.12(248)	$0.32 \pm 0.05(1.98)$	0.04 ± 0.01
0411780701*	0.89 ± 0.01	-	1.47 ± 0.01	1.11(150)	$0.28 \pm 0.05(1.22)$	$0.01^{+0.02}_{-0.05}$

Table 3. Double power-law spectral fit results (νF_{ν}) for the epochs with convex X-ray spectra. ϵ_{ν} is the photon energy in keV corresponding to the valley in the SED (equation 6). The index Γ_{com} is fixed to the value obtained from a power-law fit to the UV/optical spectra (see § 2). $F_{0.6-10 \text{ keV}}$ is the integrated flux over the energy range 0.6 to 10 keV ($10^{-11} \text{ erg cm}^{-2} \text{ s}^{-1}$). The reduced χ^2 and degrees of freedom (dof) correspond to the best fit double power-law model. κ_{lp} is the curvature of the best fit log parabola model. The Γ_{syn} and $F_{0.6-10 \text{ keV}}$ corresponding to observation 0411780701* are obtained by a simple power-law fit.

Obs. ID	$\epsilon_{\text{min,c}}$	χ^2_{red}
0158961401	0.607	1.064
0411780101	0.619	1.040
0411780201	0.654	1.128

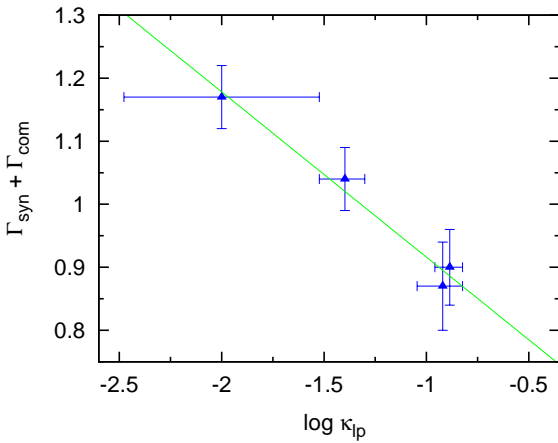


Figure 1. Scatter plot between curvature of logparabola function (κ_{lp}) with ($\Gamma_{\text{syn}} + \Gamma_{\text{com}}$) for the epochs with convex X-ray spectra. Solid green line is the best fit straight line to the data points (see text).

mands prior knowledge about the physical parameters of the source. Given a jet Doppler factor δ and a source magnetic field strength B , the characteristic mean energy change in IC/SSC scattering (Thomson regime), considering relativistic and cosmological effects, will

Table 4. Upper limit on the minimum photon energy of the Compton spectra ($\epsilon_{\text{min,c}}$) inferred by using a double power-law fit (see text).

be (Rybicki & Lightman 1986)

$$\epsilon_{\text{SSC}}(\gamma) = \left(\frac{\delta}{1+z} \right) \gamma^2 \epsilon'_{\text{syn}}, \quad (10)$$

where z is the source red shift and ϵ'_{syn} the (synchrotron) soft photon energy. The characteristic synchrotron photon energy corresponding to the electron Lorentz factor γ , as measured in the rest frame of the emitting region, is given by

$$\epsilon'_{\text{syn}}(\gamma) = \gamma^2 \left(\frac{heB}{2\pi m_e c} \right).$$

Requiring the Compton branch to extend down to at least $\epsilon_{\text{min,c}}$, i.e. $\epsilon_{\text{SSC}}(\gamma_{\text{min}}) \gtrsim \epsilon_{\text{min,c}}$, one can obtain an upper limit on γ_{min} as

$$\gamma_{\text{min}} \lesssim \left[\frac{2\pi m_e c (1+z)}{he\delta B} \epsilon_{\text{min,c}} \right]^{1/4}. \quad (11)$$

While there will be synchrotron (and correspondingly, SSC) emission below the associated γ_{min} , approximately rising as $F_{\nu} \propto \nu^{1/3}$, this will (given the SED shape of PKS 2155-304) not much alter the above noted constraint. Similarly, a lower limit on γ_{min} might be obtained in our case by requiring that IC scattering of synchrotron (SED) peak photons does not lead to a contribution in the valley energy range. This constraint can be expressed as

$$\epsilon_{\text{min,c}} < \gamma_{\text{min}}^2 \epsilon_{\text{syn,p}}, \quad (12)$$

where $\epsilon_{\text{syn,p}}$ is the observed synchrotron spectral peak energy. Hence, equations (11) and (12), suggest that the low-energy cut-

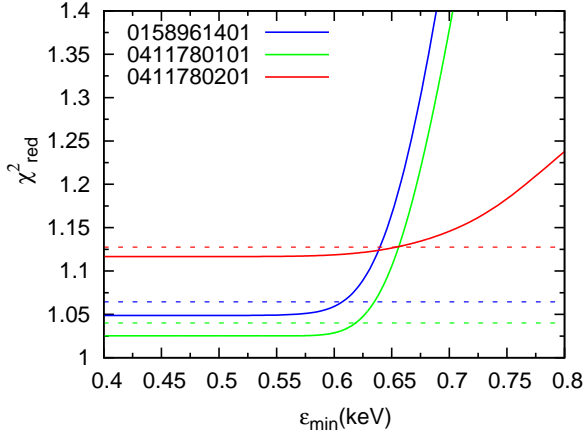


Figure 2. Variation of χ^2_{red} with ϵ_{min} for the epochs with convex X-ray spectrum. Blue, green and red lines correspond to the observation IDs 0158961401, 0411780101 and 0411780201 respectively. Dashed horizontal lines indicate 1σ confidence level.

off γ_{min} of the radiating electron distribution satisfies

$$\sqrt{\frac{\epsilon_{\text{min},c}}{\epsilon_{\text{syn},p}}} \lesssim \gamma_{\text{min}} \lesssim \left[\frac{2\pi m_e c(1+z)}{he\delta B} \epsilon_{\text{min},c} \right]^{1/4}. \quad (13)$$

The above relation implies that with suitable knowledge of δ , B and $\epsilon_{\text{syn},p}$, we can constrain γ_{min} through $\epsilon_{\text{min},c}$ obtained from the convex X-ray spectrum. As we show in Sec. 6, the heuristic arguments employed here to infer γ_{min} are supported by results based on full spectral modelling.

5.1 Kinetic Jet Power

If we consider a distribution of radiating electrons that is approximated to a power-law described by²

$$N(\gamma)d\gamma = K \left(\frac{\gamma}{\gamma_p} \right)^{-p} d\gamma; \quad \gamma_{\text{min}} < \gamma < \gamma_p, \quad (14)$$

then, given $p > 1$ and $\gamma_p \gg \gamma_{\text{min}}$, the total electron number density is dominated by the electrons with energy γ_{min} and is given by

$$N_{\text{tot}} \approx \int_{\gamma_{\text{min}}}^{\gamma_p} N(\gamma)d\gamma \approx \frac{K}{p-1} \left(\frac{\gamma_{\text{min}}}{\gamma_p} \right)^{-p+1}. \quad (15)$$

Under the heavy (e-p) jet approximation, the mass density of the jet is dominated by protons whose number density is assumed to be equal (charge-neutrality) to that of the non-thermal electrons (N_{tot}). The bulk kinetic power of the jet ($P_{\text{jet,heavy}}$) is then typically

² Broadband spectral fitting for PKS 2155-304 demands a broken power-law electron distribution and the same is considered in §6. Since the total electron number density is governed by the differential number density at γ_{min} , the consideration of a simple power-law is sufficient here.

dominated by protons (for $\gamma_{\text{min}} \ll \left(\frac{m_p}{m_e}\right)$), and if we assume them to be cold, the jet kinetic power will be

$$P_{\text{jet,heavy}} \approx \pi R^2 \Gamma^2 \beta_{\Gamma} U_p c, \quad (16)$$

where $U_p = N_{\text{tot}} m_p c^2$ is the proton energy density, R is the size of the jet region, Γ is the bulk flow Lorentz factor and $\beta_{\Gamma} = (1 - \Gamma^{-2})^{1/2}$. Using equations (13), (15) and (16), $P_{\text{jet,heavy}}$ is constrained as

$$\left[\frac{he}{2\pi m_e c(1+z)} \frac{B}{\epsilon_{\text{min},c}} \right]^{\frac{p-1}{4}} \delta^{\frac{p+7}{4}} \lesssim \zeta P_{\text{jet,heavy}} \lesssim \delta^2 \left(\frac{\epsilon_{\text{syn},p}}{\epsilon_{\text{min},c}} \right)^{\frac{p-1}{2}} \quad (17)$$

where

$$\zeta = \left(\frac{p-1}{\pi m_p c^2 R^2 K} \right) \gamma_p^{1-p},$$

and we assumed $\Gamma \approx \delta$ and $\beta_{\Gamma} \approx 1$.

For a light jet, where the energy density is dominated by electrons and positrons, the kinetic power of the jet ($P_{\text{jet,light}}$) becomes

$$P_{\text{jet,light}} \approx \pi R^2 \Gamma^2 \beta_{\Gamma} U_e c, \quad (18)$$

where U_e is the leptonic energy density given by

$$U_e \approx m_e c^2 \int_{\gamma_{\text{min}}}^{\gamma_p} \gamma N(\gamma) d\gamma \approx \frac{K \gamma_p m_e c^2}{p-2} \left(\frac{\gamma_{\text{min}}}{\gamma_p} \right)^{-p+2}, \quad (19)$$

under the approximations $\gamma_p \gg \gamma_{\text{min}}$ and $p > 2$. Hence,

$$P_{\text{jet,light}} \approx \left(\frac{p-1}{p-2} \right) \left(\frac{m_e}{m_p} \right) \gamma_{\text{min}} P_{\text{jet,heavy}}. \quad (20)$$

Using equation (13), $P_{\text{jet,light}}$ is constrained by

$$\left[\frac{he}{2\pi m_e c(1+z)} \frac{B}{\epsilon_{\text{min},c}} \right]^{\frac{p-2}{4}} \delta^{\frac{p+6}{4}} \lesssim \xi P_{\text{jet,light}} \lesssim \delta^2 \left(\frac{\epsilon_{\text{syn},p}}{\epsilon_{\text{min},c}} \right)^{\frac{p-2}{2}}, \quad (21)$$

where

$$\xi = \left(\frac{p-2}{\pi R^2 K m_e c^2} \right) \gamma_p^{1-p}. \quad (22)$$

6 BROADBAND SPECTRAL MODELLING

As noted above, estimation of the minimum available energy γ_{min} and the jet power demands knowledge of the source parameters, δ and B . In order to obtain these information, we performed a broadband spectral fitting of the SED considering both synchrotron and SSC emission processes (Sahayanathan et al. 2018). The emission from the source is imitated by assuming the emission region to be a spherical region of size R , permeated by a tangled magnetic field B and populated by a broken power-law distribution of the form

$$N(\gamma) = K \times \begin{cases} \left(\frac{\gamma}{\gamma_p} \right)^{-p}, & \gamma_{\text{min}} < \gamma < \gamma_p \\ \left(\frac{\gamma}{\gamma_p} \right)^{-q}, & \gamma_p < \gamma < \gamma_{\text{max}} \end{cases} \quad (23)$$

The Doppler factor δ determines the flux enhancement due to the relativistic motion of the emission region along the jet. The observed flux due to synchrotron and SSC emission processes, after

accounting for the relativistic and cosmological effects will be (e.g., Begelman et al. 1984; Dermer 1995)

$$F_{\text{obs}}(\epsilon) = \frac{\delta^3(1+z)}{d_L^2} V \left[j_{\text{syn}} \left(\frac{1+z}{\delta_D} \epsilon \right) + j_{\text{SSC}} \left(\frac{1+z}{\delta_D} \epsilon \right) \right] \quad (24)$$

where, j_{syn} and j_{SSC} are the synchrotron and SSC emissivities measured in the frame of emission region (e.g., Sahayanathan et al. 2018; Finke et al. 2008), d_L is the luminosity distance and V is the volume of the emission region. For the SSC emissivity, we have considered the full Klein-Nishina cross section for the scattering process. The spectrum is then essentially governed by seven source parameters namely, p , q , K , γ_p , R , B and δ . The limited information available from the optical and X-ray energies does not allow us to constrain all these parameters and hence, we impose certain conditions to determine the characteristic range of the source parameters. We assume equipartition between the emitting electron energy density and the magnetic field. This assures a minimum energy budget (Burbidge 1959) and using equation (19) we can express B as

$$B \approx \sqrt{\frac{8\pi\eta K\gamma_p m_e c^2}{(p-2)} \left(\frac{\gamma_{\text{min}}}{\gamma_p} \right)^{-p+2}}, \quad (25)$$

where $\eta = 1$ corresponds to equipartition and γ_{min} can be constrained from equation (13). The parameter γ_p determines the SED peak of the synchrotron spectral component

$$\epsilon_{\text{syn,p}} = \left(\frac{h\delta}{1+z} \right) \left(\frac{eB}{2\pi m_e c} \right) \gamma_p^2 \quad (26)$$

and $\epsilon_{\text{syn,p}}$ can be obtained from the intersection of extrapolated optical/UV and X-ray spectra. Finally, we constrain R by assuming a variability timescale, t_{var} , as

$$R \approx \frac{c}{1+z} \delta t_{\text{var}} \quad (27)$$

Along with these constraints, we also included archival γ -ray data of the source as obtained by *Fermi*-LAT for the spectral fit. Since simultaneous γ -ray observations were not available, we chose observations in 2008 (Aharonian et al. 2009) as this being the closest one available with the X-ray observation epochs (2006-2007) considered in this work. In addition, we also included 2013 γ -ray observations (Madejski et al. 2016) during which the source was found to be in its lowest flux state.

We developed a numerical code to generate the synchrotron and SSC emission spectra from the source parameters, along with the constraints discussed above. The computer routine is added as a local model in XSPEC and used to fit the optical/UV, X-ray and the archival γ -ray observations (Sahayanathan et al. 2018). The fitting procedure is performed as follows: We first fixed $t_{\text{var}} = 1$ day, $\eta = 1$ and $\epsilon_{\text{min,c}}$ to values obtained from Table 4. Following this, the best fit parameters were obtained by allowing the parameters p , q and $\epsilon_{\text{syn,p}}$ to vary within the confidence intervals obtained from the power-law/broken power-law/double power-law spectral fits to optical/UV, X-ray and γ -ray spectra; whereas, δ and B were set to vary freely. Next freezing the parameters to their best fit values except for δ and B , we obtained the confidence intervals on these two parameters. In order to obtain error in the parameters, XSPEC demands $\chi_{\text{red}}^2 < 2$. To achieve this we added 2 per cent additional error (*systematic* error in XSPEC) for the epochs corresponding to observation IDs 0158961401 and 0411780101, and 7 per cent additional error for 0411780201. The best fit source parameters corresponding to the two archival γ -ray observations are given in Table 5 and 6. Using the best fit parameters, we obtained the range of γ_{min} , $P_{\text{jet,heavy}}$ and $P_{\text{jet,light}}$ which are also provided in Table 5

and 6 (bottom). In the left panel of Figure 3, we show the best fit broadband SED along with the observed fluxes and in right panel, the XSPEC fit results with the residuals corresponding to 2008 γ -ray observation. We note that the spectral fit is very sensitive to the choice of $\epsilon_{\text{min,c}}$ or its equivalent γ_{min} . In Figure 4, we show the variation of χ^2 with γ_{min} while the rest of source parameters are fixed to their best-fit values for the spectral fit corresponding to the *XMM-Newton* observation ID 0158961401. For the best fit parameters given in Table 5, the minimum χ^2 is achieved when $\gamma_{\text{min}} \approx 330$. The required kinetic jet power for a light jet is of the order 3×10^{44} erg s $^{-1}$, and nearly an order of magnitude higher for a heavy jet. Assuming a black hole mass of $\sim 5 \times 10^8 M_{\odot}$, this would roughly correspond to levels of ~ 0.1 per cent and ~ 1 per cent of the maximum possible jet power, respectively (e.g., Katsoulakos & Rieger 2018)

Parameters	(0158961401)	(0411780101)	(0411780201)
δ	$21.19^{+0.71}_{-0.66}$	$23.94^{+0.10}_{-0.10}$	$31.37^{+1.31}_{-1.16}$
B	0.238 ± 0.013	$0.209^{+0.002}_{-0.001}$	0.114 ± 0.008
p	2.70	2.73	2.43
q	4.36	4.36	4.36
$\epsilon_{\min,c}$	0.607	0.619	0.654
$\epsilon_{\text{syn},p} (10^{-2})$	3.31	3.64	5.02
Properties			
γ_{\min}	59.40 - 328.33	67.27 - 330.45	60.61 - 364.66
$P_{\text{jet,heavy}}$	45.40 - 44.74	45.55 - 44.84	45.52 - 44.63
$P_{\text{jet,light}}$	44.41 - 44.36	44.56 - 44.46	44.56 - 44.40

Table 5. The best fit source parameters and inferred quantities of PKS 2155-304 for the three observation IDs as obtained using a synchrotron and SSC emission model. The gamma-ray reference data are from 2008 *Fermi*-LAT observations (Aharonian et al. 2009). δ : Doppler factor, B: magnetic field (Gauss), p and q : low and high energy particle spectral indices, $\epsilon_{\min,c}$: observed minimum photon energy of the Compton component (keV) (fixed to the values obtained from Table 4), $\epsilon_{\text{syn},p}$: synchrotron peak energy (keV), γ_{\min} : minimum electron energy (in units of $m_e c^2$), $P_{\text{jet,heavy}}$: jet kinetic power (log) estimated for an e-p jet (erg s^{-1}), $P_{\text{jet,light}}$: jet kinetic power (log) estimated for a light jet (erg s^{-1}). Fixed parameters are $\eta = 1$, $t_{\text{var}} = 1$ day and $\gamma_{\text{max}} = 10^7$.

Parameters	(0158961401)	(0411780101)	(0411780201)
δ	24.56 ± 0.04	26.10 ± 0.08	39.62 ± 0.06
B	0.1904 ± 0.0005	0.187 ± 0.001	0.0742 ± 0.0002
p	2.78	2.80	2.43
q	4.36	4.36	4.36
$\epsilon_{\min,c}$	0.607	0.619	0.654
$\epsilon_{\text{syn},p} (10^{-2})$	3.70	3.81	5.03
Properties			
γ_{\min}	77.70 - 334.44	92.17 - 332.36	60.55 - 382.64
$P_{\text{jet,heavy}}$	45.44 - 44.82	45.50 - 44.92	45.59 - 44.65
$P_{\text{jet,light}}$	44.50 - 44.43	44.60 - 44.52	44.61 - 44.44

Table 6. Same as in Table 5, but for gamma-ray reference data based on 2013 *Fermi*-LAT observations (Madejski et al. 2016).

7 DISCUSSION AND CONCLUSION

Our analysis shows that the convex X-ray spectra of PKS 2155-304 can be successfully interpreted as a combination of synchrotron and SSC spectral components. We demonstrate that this result along with the knowledge of source parameters can be effectively utilized to draw better constraints on the minimum energy γ_{\min} of the emitting electron distribution and the power of the blazar jet. In general, the hard X-ray emission of PKS 2155-304 is expected to reveal a convex nature irrespective of flux state. *NuSTAR* observation of the source at 3-79 keV can thus effectively probe the valley regime and provide further constraints on γ_{\min} . In the current work, however, we wanted to highlight the occasional convex spectra that have been observed in the soft X-ray regime using *XMM-Newton* observations. The constraints on γ_{\min} are derived from these epochs of convex soft X-ray spectra. The source parameters were obtained through statistical fitting of the broadband SED using synchrotron and SSC emission processes. We observed that the spectral fit is very sensitive to the parameter γ_{\min} . To explore in detail how the jet power depends on γ_{\min} , we replaced the parameter $\epsilon_{\min,c}$ with γ_{\min} in our numerical emission model and repeated the fitting procedure (as mentioned in §6). In Figure 5, we show the variations of $P_{\text{jet,heavy}}$ (solid purple line) and $P_{\text{jet,light}}$ (dashed magenta line) with respect to γ_{\min} along with the goodness-of-fit χ^2 in the bottom (solid red line). The fitting was performed on the SED correspond-

ing to the *XMM-Newton* observation ID 0158961401 along with its 2008 γ -ray reference spectrum. The horizontal red dashed line corresponds to reduced $\chi^2 = 1$ and the vertical blue dashed lines corresponds to the limiting values of γ_{\min} (Table 5). The dependence of χ^2 over γ_{\min} shown in Figure 4 satisfies the condition obtained earlier in §5 equation (13). We found that $P_{\text{jet,heavy}}$ varies more strongly with γ_{\min} than $P_{\text{jet,light}}$. Also, as γ_{\min} approaches $\left(\frac{m_p}{m_e}\right)$, $P_{\text{jet,light}} \approx P_{\text{jet,heavy}}$. Further, considering the best fit values of δ and B, the allowed range of jet power can be constrained by the gray-shaded area in figure 5.

In general, the non-availability of simultaneous γ -ray data introduces some uncertainty on the fit parameters. On the other hand, Table 5 and 6 reveal that the estimates for γ_{\min} and the jet kinetic power do not vary much for the two different gamma-ray flux states of the source. The obtained limits on γ_{\min} and jet powers may therefore be viewed as typical values for PKS 2155-304. In principle, uncertainty in the size of the emission region R could also impact these estimates. To test this, we repeated the fitting by freezing t_{var} to a predefined value while setting $\eta = 1$ and $\gamma_{\min} = 328.33$. Figure 6 shows the variation in $P_{\text{jet,light}}$ and $P_{\text{jet,heavy}}$ along with the χ^2 (bottom panel). The variation in jet power is found to be within the same order while t_{var} changes from 0.1 to 2 days. This suggests that our inferred values represent the typical parameter space of the source.

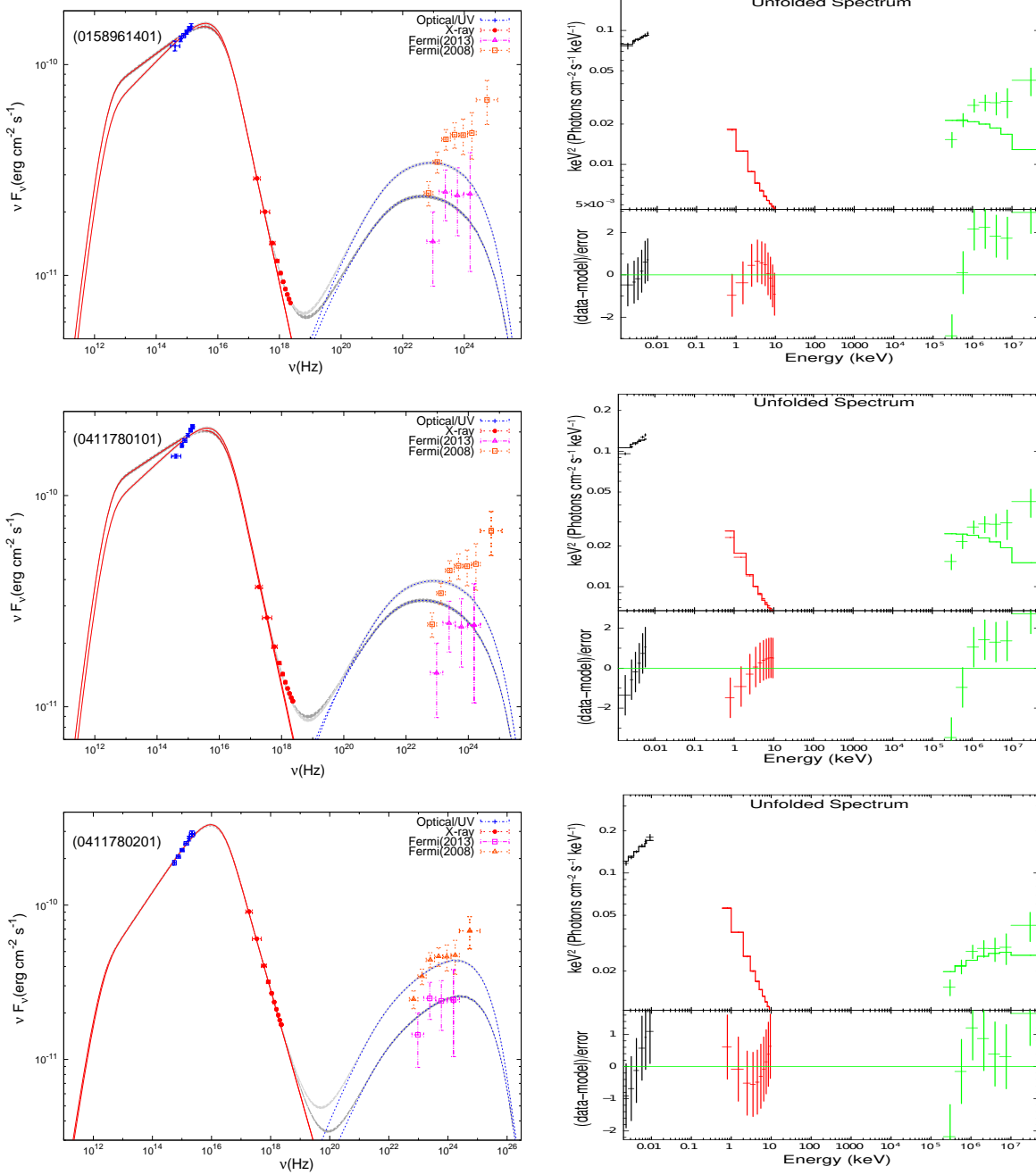


Figure 3. The best fit SEDs corresponding to three epochs with convex X-ray spectrum and the *Fermi*-LAT reference observations of the source during 2008 and 2013. The solid line represents synchrotron and the dashed line represents SSC contribution. The thick gray band represents the combined emission with the width of the band representing the systematic error added to the model. The XSPEC spectral fit, along with residual are given in the right panel corresponding to the 2008 gamma-ray observations.

The assumption of equipartition between the particle energy density and magnetic field relies on the principle that the source remains in its minimum energy state. However, there is no consensus that this condition should be satisfied rigorously. For instance, the chosen equipartition condition assumes that the radiating particle distribution largely determines the total electron density. However, protons may also carry significant energy (while still being radiatively inefficient) and for such conditions $\eta \neq 1$. Similarly, when the electrons undergo non-radiative losses (e.g., adiabatic expansion) along with synchrotron losses, the equipartition condition may not be satisfied (Lefa et al. 2011). Besides

this, broadband spectral fitting of blazar SED by synchrotron and IC emission also indicates significant deviation from equipartition (e.g., Tavecchio & Ghisellini 2016). To study the dependence of jet power on the assumed equipartition, we also repeated fitting for different values of η keeping $t_{\text{var}} = 1$ and $\gamma_{\text{min}} = 328.33$. We found that the jet power varies by a factor of 10 as η varies from 0.1 to 10. This large variation advocates η to be an important parameter in deciding the energetics of the source.

It is widely accepted that the broadband non-thermal emission from blazars originates from relativistic jets. The formation and collimation of these jets, however, still remains an unresolved puzzle.

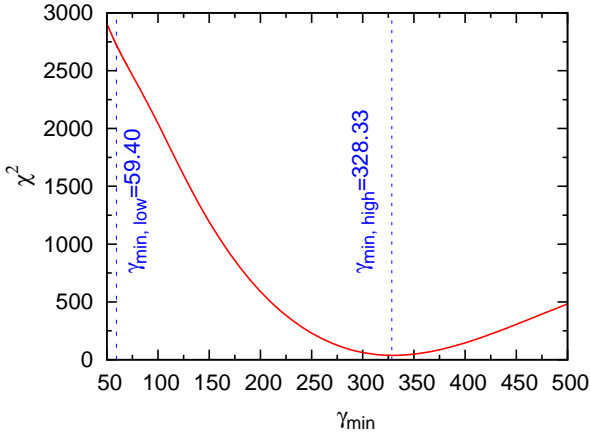


Figure 4. Variation of χ^2 of the spectral fit for the best fit parameters given in Table 5 (observation ID 0158961401) with change in γ_{\min} . The dashed vertical blue lines denote lower and upper limit on γ_{\min} (cf. eq. [13]), respectively.

zle. Assumptions regarding this include jets that are solely powered by the accretion disk (Blandford & Payne 1982) or with additional energy derived from the spin of the black hole (Blandford & Znajek 1977). In both the cases, a crucial role is played by the magnetic field transporting power from the black hole/accretion disk to the jet (e.g., Tchekhovskoy et al. 2011; Katsoulakos & Rieger 2018). Since the magnetic field is thought to be supported by accretion, the jet power is supposed to be correlated to accretion power. Requiring that the power of heavy jets satisfy the linear regression (Ghisellini et al. 2014)

$$\log P_{\text{jet,heavy}} = 0.92 \log(\dot{M} c^2) + 4.09 \quad (28)$$

would imply accretion rates up to $\dot{M} \approx 0.02 M_{\odot}/\text{yr}$, or $\sim 2 \times 10^{-3} \dot{M}_{\text{Edd}}$ for a black hole of mass $5 \times 10^8 M_{\odot}$, which seems feasible.

Our SED modelling favours a minimum Lorentz factor for the non-thermal electron distribution of $\gamma_{\min} \gtrsim 60$, with a strong preference for a value around $\gamma_{\min} \approx 330$ (§6). Since radiative cooling is slow for the inferred parameters, it seems likely that γ_{\min} has to be related to the underlying particle acceleration mechanism. In general, diffusive shock acceleration is commonly regarded as one of the most promising mechanisms (e.g., Kino & Takahara 2004; Rieger et al. 2007; Giannios & Spitkovsky 2009). Shocks are known to convert the kinetic energy of the incoming flow to the thermal energy, represented by a relativistic Maxwellian particle distribution peaking at energy $\gamma_p = 2\theta$, where $\theta \equiv kT$, along with a non-thermal, power-law type component above γ_p . Here, k is the Boltzmann constant and T is the effective plasma temperature. For a pure electron-positron plasma this suggests $\gamma_{\min} \sim \Gamma_s$ for the downstream particle distribution, where Γ_s is the relative Lorentz factor between the shocked and the unshocked fluid. For a pure electron-proton (e-p) plasma, on the other hand, γ_{\min} depends on the degree of thermal coupling between electrons and protons. For $T_e = \zeta T_p$, where T_e and T_p are the electron and proton plasma temperatures,

and $\zeta \leq 1$, one finds

$$\gamma_{\min} = 2 \left(\frac{m_p}{m_e} \right) \Gamma_s \frac{\zeta}{1 + \zeta}. \quad (29)$$

In the case of inefficient thermal coupling, $\zeta \approx \left(\frac{m_e}{m_p} \right)$ and hence, $\gamma_{\min} \sim 2\Gamma_s$. On the other hand, for strong thermal coupling $\zeta \approx 1$ and $\gamma_{\min} \sim \left(\frac{m_p}{m_e} \right) \Gamma_s$. For the jet in blazars, such as PKS 2155-304, one typically has $\Gamma_s \sim \Gamma$ ($\approx \delta$) or $\Gamma_s \sim$ a few, for acceleration at external or internal shocks respectively. Our broadband spectral fitting assuming synchrotron and SSC emission mechanisms suggests $\delta \sim 20$ (Table 5). Hence, our constraint on γ_{\min} would tend to disfavour a pure e^+e^- plasma, while our best-fit value $\gamma_{\min} \approx 330$ would only be consistent with a pure e-p plasma composition in case of some reduced thermal coupling at mildly relativistic internal shocks. While PIC simulations of unmagnetized, collisionless relativistic electron-ion shocks (Spitkovsky 2008; Sironi et al. 2013; Vanthieghem et al. 2020) indicate a thermal coupling that is somewhat stronger ($\zeta \sim 0.2 - 0.5$), variations in magnetization, shock speed and orientation may possibly explain the difference. If confirmed, this would tend to favour an e-p composition, at least for the X-ray emitting part of the jet.

Our results show that the convex X-ray spectra of blazars offer important insights into the source energetics as well as the matter content of jets. As indicated above, a crucial uncertainty in the present work relates to the equipartition parameter η . An appropriate value of η could be obtained through a detailed study of the particle acceleration process. For instance, if the particles are energized through shock acceleration then a fraction of the shock energy is spent in enhancing the magnetic field. A clear understanding about the energy budget involved demands detailed numerical simulation of relativistic MHD jet flow. This should be further supplemented with detailed spectral and temporal behaviour which can provide inputs/tests for the simulations. One such information can be the simultaneous broadband SED extending up to GeV/TeV gamma-ray energies during lower flux states, supplemented with the temporal behavior of the source. Future upcoming ground-based Cherenkov Telescope Array observations will have the capability to gather information from the source at VHE energies, even at low flux states. This along with the inputs from other wavebands could play an important role in providing valuable information regarding the source energetics.

ACKNOWLEDGEMENTS

Useful comments by the anonymous referee are gratefully acknowledged. This research is based on observations obtained with the *XMM-Newton* satellite, an ESA science mission with instruments and contributions directly funded by ESA member states and NASA. This work has made use of the NASA/IPAC Extra Galactic Database operated by Jet Propulsion Laboratory, California Institute of Technology and the High Energy Astrophysics Science Archive Research Center (HEASARC) provided by NASA's Goddard Space Flight Center. JKS thanks Jithesh V and Zahir Shah for useful discussions. JKS wishes to thank UGC-SAP and FIST 2 (SR/FIST/PS1-159/2010) (DST, Government of India) for the research facilities in the Department of Physics, University of Calicut. JKS is grateful to the University Grants Commission for the financial support through the RGNF scheme.

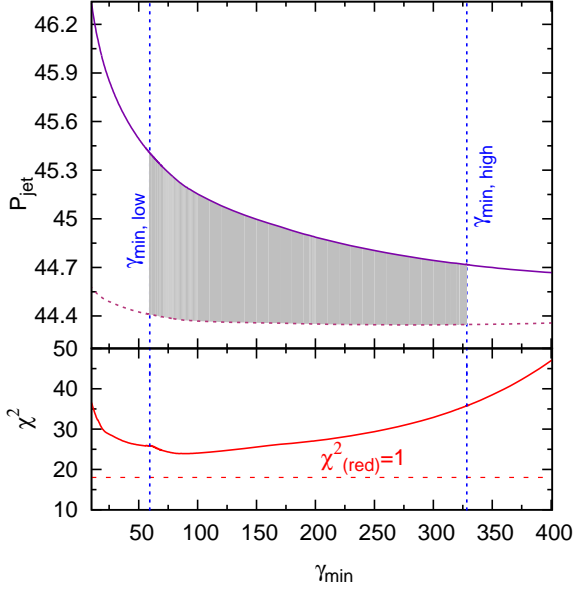


Figure 5. Variation in jet power as a function of minimum electron energy γ_{\min} (expressed in units of $m_e c^2$) for the observation ID 0158961401. The solid purple line corresponds to $P_{\text{jet,heavy}}$ and the dashed magenta line corresponds to $P_{\text{jet,light}}$. The red solid line in the bottom panel is the best fit χ^2 for different γ_{\min} values and the dashed line denotes $\chi_{\text{red}}^2 = 1$. The vertical blue dashed lines represent the limiting values of γ_{\min} . The gray shaded area is the allowed ranges of jet kinetic power.

DATA AVAILABILITY

The data underlying this article are publicly available from the HEASARC³ and the *Fermi*-LAT⁴ archives.

REFERENCES

- Abdalla H., et al., 2020, *A&A*, **639**, A42
 Abdo A. A., et al., 2010, *ApJ*, **716**, 30
 Aharonian F., et al., 2007, *ApJ*, **664**, L71
 Aharonian F., et al., 2009, *ApJ*, **696**, L150
 Arnaud K. A., 1996, in Jacoby G. H., Barnes J., eds, *Astronomical Society of the Pacific Conference Series Vol. 101, Astronomical Data Analysis Software and Systems V*. p. 17
 Begelman M. C., Blandford R. D., Rees M. J., 1984, *Reviews of Modern Physics*, **56**, 255
 Begelman M. C., et al., 1987, *ApJ*, **322**, 650
 Bhagwan J., Gupta A. C., Papadakis I. E., Wiita P. J., 2014, *MNRAS*, **444**, 3647
 Blandford R. D., Payne D. G., 1982, *MNRAS*, **199**, 883
 Blandford R. D., Znajek R. L., 1977, *MNRAS*, **179**, 433
 Burbidge G. R., 1959, *ApJ*, **129**, 849
 Celotti A., Ghisellini G., 2008, *MNRAS*, **385**, 283

³ <https://heasarc.gsfc.nasa.gov/>

⁴ <https://fermi.gsfc.nasa.gov/ssc/data/access/>

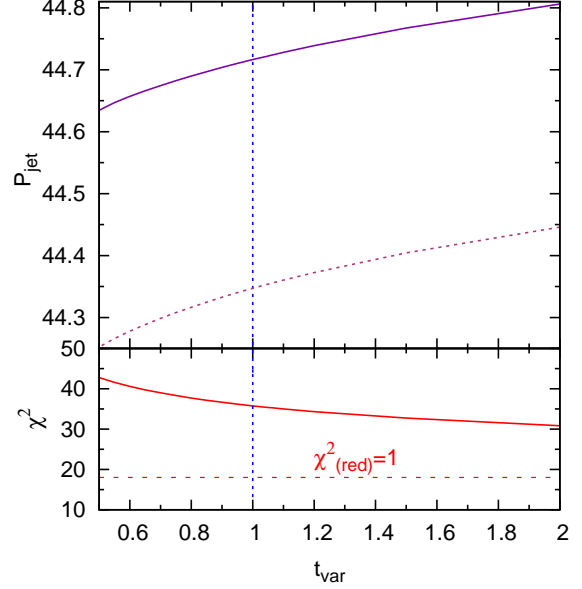


Figure 6. Variation in jet power for a range of variability time-scale t_{var} (in days) corresponding to the observation ID 0158961401. The solid purple line corresponds to $P_{\text{jet,heavy}}$ and the dashed magenta line corresponds to $P_{\text{jet,light}}$. The red solid line in the bottom panel is the best fit χ^2 for different t_{var} values and the dashed line denotes $\chi_{\text{red}}^2 = 1$. The vertical blue dashed line represents $t_{\text{var}} = 1$ day.

- Dermer C. D., 1995, *ApJ*, **446**, L63
 Dermer C. D., Atayan A. M., 2002, *ApJ*, **568**, L81
 Dermer C. D., Schlickeiser R., 1993, *ApJ*, **416**, 458
 Finke J. D., Dermer C. D., Böttcher M., 2008, *ApJ*, **686**, 181
 Fossati G., Maraschi L., Celotti A., Comastri A., Ghisellini G., 1998, *MNRAS*, **299**, 433
 Gaur H., Chen L., Misra R., Sahayanathan S., Gu M. F., Kushwaha P., Dewangan G. C., 2017, *ApJ*, **850**, 209
 Gaur H., Mohan P., Wiercholska A., Gu M., 2018, *MNRAS*, **473**, 3638
 Ghisellini G., Tavecchio F., Maraschi L., Celotti A., Sbarrato T., 2014, *Nature*, **515**, 376
 Ghisellini G., Righi C., Costamante L., Tavecchio F., 2017, *MNRAS*, **469**, 255
 Giannios D., Spitkovsky A., 2009, *MNRAS*, **400**, 330
 Goswami P., Sahayanathan S., Sinha A., Gogoi R., 2020, *MNRAS*, **499**, 2094
 IceCube Collaboration et al., 2018, *Science*, **361**, eaat1378
 Jagan S. K., Sahayanathan S., Misra R., Ravikumar C. D., Jeena K., 2018, *MNRAS*, **478**, L105
 Kataoka J., Stawarz L., 2016, *ApJ*, **827**, 55
 Katsoulakos G., Rieger F. M., 2018, *ApJ*, **852**, 112
 Kino M., Takahara F., 2004, *MNRAS*, **349**, 336
 Kirk J. G., Mastichiadis A., 1999, *Astroparticle Physics*, **11**, 45
 Kirk J. G., Rieger F. M., Mastichiadis A., 1998, *A&A*, **333**, 452
 Kusunose M., Takahara F., 2018, *ApJ*, **861**, 152
 Lefa E., Rieger F. M., Aharonian F., 2011, *ApJ*, **740**, 64
 Madejski G. M., et al., 2016, *ApJ*, **831**, 142
 Maraschi L., Ghisellini G., Celotti A., 1992, *ApJ*, **397**, L5
 Marscher A. P., Gear W. K., 1985, *ApJ*, **298**, 114

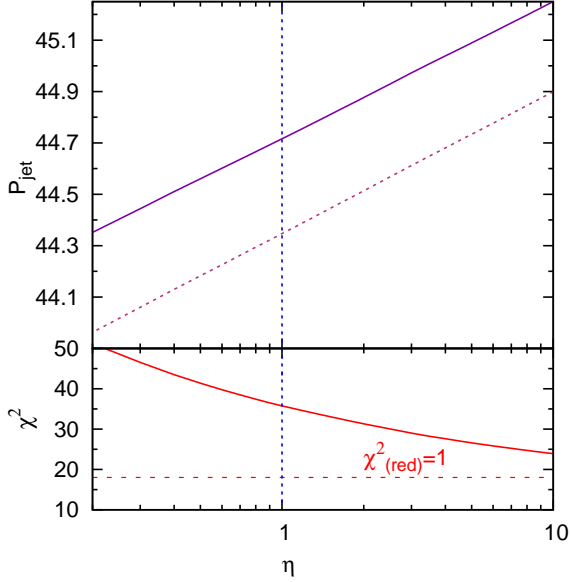


Figure 7. Variation in jet power as a function of the equipartition parameter η corresponding to the observation ID 0158961401. The solid purple line corresponds to $P_{\text{jet,heavy}}$ and the dashed magenta line corresponds to $P_{\text{jet,light}}$. The red solid line in the bottom panel is the best fit χ^2 for different η values and the dashed line denotes $\chi_{\text{red}}^2 = 1$. The vertical blue dashed line represents $\eta = 1$.

- Massaro E., Perri M., Giommi P., Nesci R., Verrecchia F., 2004, *A&A*, [422, 103](#)
- Massaro F., Tramacere A., Cavaliere A., Perri M., Giommi P., 2008, *A&A*, [478, 395](#)
- Moderski R., Sikora M., Coppi P. S., Aharonian F., 2005, *MNRAS*, [363, 954](#)
- Ostrowski M., 2000, *MNRAS*, [312, 579](#)
- Padovani P., Giommi P., 1995, *ApJ*, [444, 567](#)
- Press W. H., Teukolsky S. A., Vetterling W. T., Flannery B. P., 1992, Numerical recipes in FORTRAN. The art of scientific computing
- Reimer A., Böttcher M., 2013, *Astroparticle Physics*, [43, 103](#)
- Rieger F. M., Volpe F., 2010, *A&A*, [520, A23](#)
- Rieger F. M., Bosch-Ramon V., Duffy P., 2007, *Ap&SS*, [309, 119](#)
- Rybicki G. B., Lightman A. P., 1986, Radiative Processes in Astrophysics
- Sahayanathan S., Sinha A., Misra R., 2018, *Research in Astronomy and Astrophysics*, [18, 035](#)
- Schlafly E. F., Finkbeiner D. P., 2011, *ApJ*, [737, 103](#)
- Schlickeiser R., 1985, *A&A*, [143, 431](#)
- Seaton M. J., 1979, *MNRAS*, [187, 73P](#)
- Sironi L., Spitkovsky A., Arons J., 2013, *ApJ*, [771, 54](#)
- Spitkovsky A., 2008, *ApJ*, [673, L39](#)
- Stawarz Ł., Petrosian V., 2008, *ApJ*, [681, 1725](#)
- Tagliaferri G., et al., 2000, *A&A*, [354, 431](#)
- Tanihata C., Takahashi T., Kataoka J., Madejski G. M., 2003, *ApJ*, [584, 153](#)
- Tavecchio F., Ghisellini G., 2016, *MNRAS*, [456, 2374](#)
- Tavecchio F., Ghisellini G., Guetta D., 2014, *ApJ*, [793, L18](#)
- Tehekhsokoy A., Narayan R., McKinney J. C., 2011, *MNRAS*, [418, L79](#)
- Tramacere A., Massaro F., Cavaliere A., 2007, *A&A*, [466, 521](#)
- Tramacere A., Massaro E., Taylor A. M., 2011, *ApJ*, [739, 66](#)
- Vanthieghem A., Lemoine M., Plotnikov I., Grassi A., Grech M., Gremillet

- L., Pelletier G., 2020, *Galaxies*, [8, 33](#)
- Wierzcholska A., Wagner S. J., 2016, *MNRAS*, [458, 56](#)
- Zdziarski A. A., Bottcher M., 2015, *MNRAS*, [450, L21](#)
- Zhang Y. H., 2008, *ApJ*, [682, 789](#)

This paper has been typeset from a $\text{\TeX}/\text{\LaTeX}$ file prepared by the author.